Numerical investigation of some mathematical models for the COVID-19

Siphamandla Khumalo (siphamandla@aims.ac.za)
African Institute for Mathematical Sciences (AIMS)

Supervised by: Professor Justin B. Munyakazi
University of Western Cape, South Africa

22 September 2020

Submitted in partial fulfillment of a structured masters degree at AIMS South Africa

Abstract

In this paper, we construct nonstandard finite difference schemes for the numerical solutions of two COVID-19 mathematical models proposed recently by Yang and Wang (2020) and Anguelov et al. (2020). We show that the nonstandard finite difference schemes are dynamically consistent with the continuous model. Simulation of the constructed nonstandard finite difference schemes on Wuhan City and South Africa data respectively to replicate simulation of the continuous system.

Keywords: COVID-19, dynamical systems, nonstandard finite method, dynamical consistency, positivity, disease-free equilibrium.

Declaration

I, the undersigned, hereby declare that the work contained in this research project is my original work, and that any work done by others or by myself previously has been acknowledged and referenced accordingly.

Siphamandla Khumalo, 22 September 2020

Contents

1. Introduction

1.1 Background on COVID-19

An outbreak of respiratory illness believed to have a zoonotic origin is traced to originate in Wuhan City in central China in December 2019. According to Li et al. (2020), 55% of the first 425 confirmed cases were associated with a marketplace. Historically, this is not the first attack of coronavirus. According to Yang and Wang (2020), in 2002, the Severe Acute Respiratory Syndrome coronavirus (SARS-CoV) spreads to 37 countries and in 2012 the Middle East Respiratory Syndrome coronavirus (MERS-CoV) spreads to 27 countries. COVID-19 is the third zoonotic human coronavirus to emerge and as of July 20, 2020, there are 213 countries and territories around the world where COVID-19 has spread (Uddin et al., 2020) and no antiviral drugs or vaccine have been developed yet.

Symptoms of COVID-19 infection according to Muhammad et al. (2020) are believed to be:

- Dry cough, fever, fatigue, shortness of breath or difficulty breathing, and bilateral lung infiltration in severe cases
- Repeated shaking with chills, muscle pain, headache, sore throat, the new loss of taste or smell, and many more.

Most of these symptoms are similar to SARS-CoV and MERS-CoV infections. The full list of symptoms for COVID-19 is found in Wang et al. (2020). Clinical evidence shows that the incubation period of COVID-19 varies from 2 up to 14 days maximum. According to Rothe et al. (2020), during this period, the infected individual may not show any symptoms and may not be aware of their infection, but is capable of spreading the disease to susceptible population. Infection in several countries was found to be increasing exponentially at the start of the outbreak as evidenced by many studies.

The World Health Organization (WHO) declared the outbreak of the novel coronavirus a Global Public Health Emergency of International Concern on January 30, 2020. Following this situation, each country had to implement control measures according to their specific realities. Intervention strategies (such as intensive contact tracing followed by quarantine and isolation) were then implemented to reduce and control the spread of the infection whose reproduction number was initially found to be as high as 6.47 in Wuhan City as reported by Imai et al. (2020).

Other interventions such as social distancing, hand sanitisation and wearing of face masks were gradually implemented to further curb the severity of the epidemics. Further, most of the countries affected by the virus experienced lockdown. From the data, when COVID-19 was declared a pandemic by WHO, many mathematical models (Yang et al. (2020), Tu et al. (2020), Batista (2020), Victor (2020), Yang and Wang (2020), Anguelov et al. (2020)) have been developed in order to understand the mechanisms of the spread of this infection and how different control measures help reduce the impact of the disease.

1.2 Mathematical models

Mathematical analysis and modeling have become central to infectious disease epidemiology. The significant rise of the mathematical epidemiology has been an inclusion of mathematical models in estimating the parameters of these models (Grassly and Fraser, 2008) and also used to extrapolate from epidemiology data in predicting risk. Mathematical models are extensively used to study the disease transmission dynamics in human populations.

Epidemiology models use mathematical approaches/techniques to understand the spread of contagious diseases in the population. Mathematical modeling in epidemiology gives us comprehension of the disease transmission routes and then recommends methods of control. Models also help to identify measurement errors in the experimental data. In the unavailability of genuine data, mathematical models help formulate hypotheses, inform data-collection strategies, and determine sample sizes/spread depending on the objective (Grassly and Fraser, 2008).

All mathematical models of necessity make use of simplified assumptions, and as a result, there is a trade-off between biological accuracy and mathematical tractability. In this field of study, there are also well-established mathematical studies concerned with dynamic models of populations in which all individuals are no longer treated identically to one another. Individuals differ in the ways they interact with their physical environment and with other individuals (Thieme, 2003).

Mathematical models can be used to associate the biological activities of transmission and the arising dynamics of infection at the population level. An epidemic can be traced by enumerating the cycle of infection (who infected who and when) (Grassly and Fraser, 2008).

The terms **discrete** and **continuous** in many studies are referred to as representations of time. Models of time-related are formulated as continuous time or discrete time dynamical systems. Continuous model state variables interchanges in a steady way not instantaneously from state to state. These typical models are usually, although not exclusively constructed as differential equations, where a discrete model, is a model composed as a dynamical complex having a countable time base (Barto, 1991).

1.3 Finite difference methods

The idea of the finite difference (FD) method is to minimize the complication that arises when continuous functions are represented by an array of samples spaced in intervals (finite). The FD schemes solve problems presented in the form of differential equations. These schemes are then mostly analyzed for efficiency and accuracy by theoretical means (Manning and Margrave, 2020).

Rao et al. (2018) mentioned that understanding the solution's behavior for FD methods is quite useful in restraining the rise of undesired populations. In many studies the significance of designing a nonstandard finite difference (NSFD) scheme has been to approximate the continuous system in a finite time intervals, illustrating the use of dynamical consistency (DC) properties and its convergence (Mickens, 2005b). In many applications standard finite difference (SFD) methods require the use of a very small step size which, unfortunately, increases round-off errors and computational complexities. This restriction on the step size does not apply on the NSFD methods (R.Anguelov et al., 2011).

Thus, a complete discretization aid to master the behavior of the continuous system based on distinct data sets, such discrete models of the form tend to be close to actuality (Rao et al., 2018). The discrete models have been established for a wide range of non-linear dynamical systems, such as singular boundary value problems expressed in cylindrical or spherical coordinates, the dynamics of HIV transmission, modified linear heat/diffusion transport problems, (Mickens, 2005a).

Mickens (2005b) defines the NSFD scheme as follows:

1 Definition. *A FD scheme is said to be a NSFD scheme, if the following properties hold true,*

1. *In the discretized differential system, the denominator is substituted by a non-negative function* ϕ

such that

$$\frac{df(t)}{dt} = \frac{f(t+h) - f(t)}{\phi(h)} + \mathcal{O}(\phi(h)) \qquad \text{as } h \to 0, \tag{1.3.1}$$

where h is the time step size (Δt), $f(t) \in \mathbb{C}^n(\mathbb{R})^n$, and $\phi(h)$ is sometimes called the denominator function, which is real-valued function and satisfies

$$\phi(h) = h + \mathcal{O}(h^2), \forall\ h > 0.$$

2. *Addition: non- linear terms that exist in the differential are approximated in a non-local technique by a satisfactory function of a mesh of various points (Sunday and Agbataobi, 2019).*

   Example:

$$\begin{aligned} y^2 &\to y_k y_{k+1}, \\ y^2 &\to y_{k-1} y_k, \\ y^3 &\to y_{k-1} y_k y_{k+1}, \\ y^3 &\to y_k^2 y_{k+1}. \end{aligned}$$

1 Example. *To illustrate the use of DC, Mickens (2005b) considered the initial-value problem*

$$\frac{du}{dt} = -au, \qquad u(0) = u_0, \qquad \text{where } a \text{ is a positive parameter.} \tag{1.3.2}$$

Solutions $u(t) = u_0 e^{-at}$ to Equation (1.3.2) have the following properties:

- *Property 1 - $u(t) = 0$ is a fixed point,*
- *Property 2 - given $u_0 \neq 0$, then $u_0 u(t) > 0$ for all $t > 0$,*
- *Property 3 - $u(t)$ monotonically decreases in magnitude to zero for any $u_0 \neq 0$.*

A SFD scheme for System (1.3.2) is

$$\frac{u_{k+1} - u_k}{h} = -au_k,$$

or

$$u_{k+1} = u_k(1 - ah). \tag{1.3.3}$$

In Equation (1.3.3), an amplitude term $(1 - ah)$ is not always positive for different values of h, which implies that u_{k+1} oscillate if $h > \frac{1}{a}$ (giving positive and negative values) to an exact solution of Equation (1.3.2), thus, the DC property is violated.

Now to determine NSFD method for Equation (1.3.2), we set the following determinant to zero:

$$\begin{vmatrix} u_k & u(t_k) \\ u_{k+1} & u(t_{k+1}) \end{vmatrix} = 0,$$

where u_k and u_{k+1} are real-values, normalizing the function $u(t_k)$ and $u(t_{k+1})$, respectively. For Equation (1.3.2), we have,

$$\begin{vmatrix} u_k & e^{-at_k} \\ u_{k+1} & e^{-at_{k+1}} \end{vmatrix} = e^{-at_k} \begin{vmatrix} u_k & 1 \\ u_{k+1} & e^{-ah} \end{vmatrix} = 0.$$

It follows that

$$u_{k+1} = e^{-ah}u_k,$$

which can be rewritten as

$$u_{k+1} - u_k = e^{-ah}u_k - u_k,$$

or

$$u_{k+1} - u_k = -a\frac{(1 - e^{-ah})u_k}{a}.$$

This leads to

$$\frac{u_{k+1} - u_k}{\phi} = -au_k.$$

Thus, we obtain the NSFD scheme

$$u_{k+1} = u_k - a\phi u_k, \quad \textit{where} \quad \phi = \frac{(1 - e^{-ah})}{a}. \tag{1.3.4}$$

It is to be noted that Equation (1.3.4), the difference equation, has the same solution, as Equation (1.3.2), with a fixed point being $u(t) = 0$. Given that $u_0 \neq 0$, then $u_0 u(t) > 0$ for $t > 0$, and u_{k+1} is monotonically decreasing in magnitude to zero for any $u_0 \neq 0$, consequently the DC properties for NSFD scheme holds. The convergence and the absolute error of the schemes are illustrated by Figure 1.1, where the graphs were computed setting values $(a, u_0, h) = (4, 20, 0.5)$ and $t = [0, 5]$.

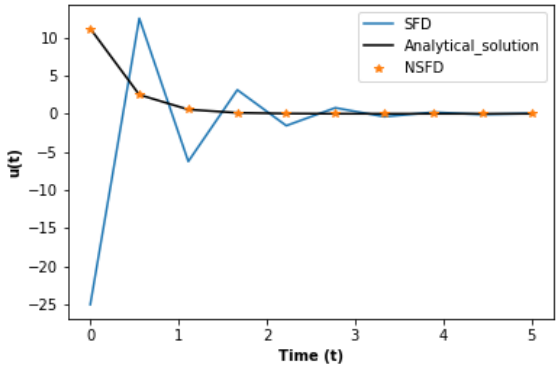

(a) Graph of the exact solution, and numerical solutions via SFD and NSFD schemes

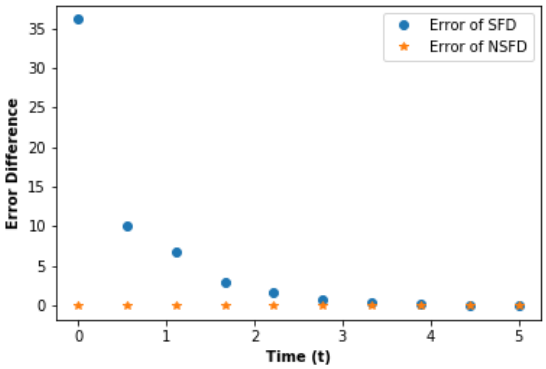

(b) Absolute error of SFD and NSFD schemes

Figure 1.1: Comparison of SFD and NSFD schemes.

Table 1.1: Error of SFD and NSFD schemes for Example 1.

Error of SFD scheme	*Error of NSFD scheme*
36.15650801	*1.77635684e-15*
10.01064658	*1.77635684e-15*
6.80544983	*5.55111512e-16*
3.00106239	*1.66533454e-16*
1.59015422	*4.85722573e-17*
0.77507951	*1.21430643e-17*
0.39200182	*3.68628739e-18*
0.19500529	*9.75781955e-19*
0.0977248	*2.57498016e-19*
0.04881283	*6.43745040e-20*

From Figure 1.1(a), the SFD scheme does not decrease monotonically, in fact it oscillates to exact solution, while NSFD decreases monotonically in magnitude to zero as shown in Figure 1.1(b) as well as in Table 1.1.

NSFD scheme Solution (1.3.4) can be said to be an exact solution, since the rounding error is $< 10^{-15}$*, while for SFD scheme the error difference is too big, as shown in Table 1.1. For SFD scheme the values of* h *are restricted, oscillating to zero but not monotonically decreasing, Thus we can conclude that NSFD is better suited to approximate the solution of ordinary differential equation (ODE) compared to that of the SFD method for any value of* h*.*

1.4 Objective

In this paper, we consider two mathematical models for the spread of COVID-19. We aim at constructing NSFD schemes for these models. We show that the proposed schemes are dynamically consistent with the corresponding continuous models. We use the NSFD schemes to investigate the spread of COVID-19 using Wuhan City and South Africa data.

The rest of this paper is organized as follows. In Section 2 we describe the two mathematical models for the spread of COVID-19. We present assumptions, flow diagrams and equations. Equilibrium analysis is also performed for one model. We devote Section 3 to the construction of NSFD schemes. Therein, we also verify their dynamical consistency. In Section 4 we present numerical results obtained via simulations using the constructed NSFD schemes. We show that results via NSFD schemes compare well with those obtained using the continuous models. In Section 5, we conclude the paper with some discussions based on our objectives and results.

2. Two mathematical models for the spread of COVID-19

In this section, we introduce two mathematical models for the transmission dynamics of COVID-19.

2.1 The SEIR model of Yang and Wang (2020)

2.1.1 SEIR continuous model.

There are four existence compartments of SEIR: Susceptible $S(t)$, Exposed $E(t)$, Infected $I(t)$, Recovery $R(t)$, and Yang and Wang (2020) considered that the virus can be transmitted through an environmental contract which is represented by the concentration of the coronavirus $V(t)$. This mathematical model for COVID-19 contains numerous transmission routes, incorporating the environment-to-human and human-to-human routes. An individual in class S may be infected through contact with a contaminated environment, with an individual who is contagious but asymptomatic, or who is contagious and symptomatic. The rate of infection (transmission rates) depends on the epidemiological levels and environmental conditions changing with time. When the rate of infection is high, necessity measures are taken to decrease an average transmission rate.

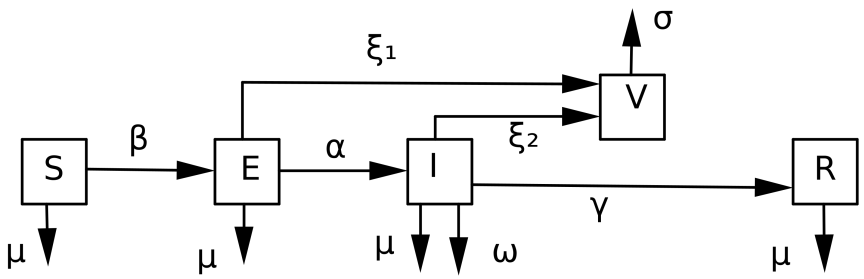

Figure 2.1: Compartmental representation of infections: SEIR model with exposed and infected contributing to environment. Boxes represents the epidemiological classes and arrows identify the processes governing transitions.

Figure 2.1 show the flow process of infection from class S to class R, where individual belonging in class S are not infected, which they attained the disease at a rate β (transmission rate), and move to class E, an incubation phase (α), where individuals are infected, but the virus is yet infectious (Zhen et al., 2016). The exposed and infected individual then contributes to the environmental reservoir with the rates ξ_1 and ξ_2 respectively. Infected individuals in class I, eventually recover at a rate γ, acquiring immunity adding to the recovery class R, or result in death either with a natural death rate μ or disease death rate ω.

The mathematical representation for the time evolution of the spread of the disease uses a system of five coupled ODEs including $V(t)$ to illustrate how the compartment changes with time, as shown in

Figure 2.1 (Mickens, 2010). The SEIR mathematical model representation is given by,

$$\begin{aligned}
\frac{dS}{dt} &= \wedge - \beta_E(E)SE - \beta_I(I)SI - \beta_V(V)SV - \mu S,\\
\frac{dE}{dt} &= \beta_E(E)SE + \beta_I(I)SI + \beta_V(V)SV - (\alpha+\mu)E,\\
\frac{dI}{dt} &= \alpha E - (\omega+\gamma+\mu)I,\\
\frac{dR}{dt} &= \gamma I - \mu R,\\
\frac{dV}{dt} &= \xi_1 E + \xi_2 I - \sigma V.
\end{aligned} \tag{2.1.1}$$

The parameter $\wedge$ indicates the population influx, μ represents the natural death rate of humans, α^{-1} is the incubation period between the exposed and infection, ω is the diseases-induced death rate, γ is the rate of recovery from infection, ξ_1 and ξ_2 are the rate of the exposed and infected individuals contributing the coronavirus to the environmental reservoir, and σ is the eradicating rate of the coronavirus from the reservoir. The parameters β_E and β_I represents the direct human-human transmission rates between the exposed and susceptible individuals and between the infected and susceptible individuals, respectively, and the function β_V represents the indirect environment-to-human transmission rate. Both μ and ω are (death rates), natural death rate and diseases death rate respectively (Yang and Wang, 2020). Note that the parameters $(\mu, \gamma, \omega, \sigma, \alpha)$ are taken to be positive.

Yang and Wang (2020) assumed that: the values of E, I, and V stimulate strong control that could reduce the transmission rates then, and further assumed that $\beta_E(E)$, $\beta_I(I)$,and $\beta_V(V)$ are non-increasing functions. Specifically,

$$\beta_E(E), \quad \beta_I(I), \quad \beta_V(V) \quad \text{are all positive,} \tag{2.1.2}$$

such that,

$$\beta_E^{'}(E) \leq 0, \quad \beta_I^{'}(I) \leq 0, \quad \beta_V^{'}(V) \leq 0.$$

1 Theorem. *Let the compartment of classes $S(t)$, $E(t)$, $I(t)$, $R(t)$ and $V(t)$ be solution to System (2.1.1), which is satisfied by conditions and Assumptions (2.1.2). Then all the compartment with respect to t are non-negative and bounded for all $t \geq 0$ (Xu and Geng, 2017).*

2.1.2 Equilibrium analysis.

2 Definition. *Stability of disease free equilibrium, E_f.*

At the disease-free equilibrium state, we have the absence of infection. Thus, all the compartment which comprises of the infections are zero and the population comprises of susceptible individual (Bawa et al., 2013).

2 Theorem. *A disease-free equilibrium state of this model exists at the point*

$$E_f = (S_0, E_0, I_0, R_0, V_0) = (\frac{\wedge}{\mu}, 0, 0, 0, 0).$$

Proof. In Equation (2.1.1), we set

$$\frac{dS}{dt} = \frac{dE}{dt}, \frac{dI}{dt} = \frac{dR}{dt} = \frac{dV}{dt} = 0.$$

Then,

$$(\beta_E(E)E + \beta_I(I)I + \beta_V(V)V)S - (\alpha + \mu)E = 0, \tag{2.1.3}$$
$$\wedge -(\beta_E(E)E - \beta_I(I)I - \beta_V(V)V - \mu)S = 0, \tag{2.1.4}$$
$$\alpha E - (\omega + \gamma + \mu)I = 0, \tag{2.1.5}$$
$$\gamma I - \mu R = 0, \tag{2.1.6}$$
$$\xi_1 E + \xi_2 I - \sigma V = 0. \tag{2.1.7}$$

Solving Equations (2.1.5), (2.1.6) and (2.1.7), we have:

$$E = \frac{\omega + \gamma + \mu}{\alpha} I, \qquad R = \frac{\gamma}{\mu} I, \quad \text{and} \quad V = \frac{\xi_1(\omega + \gamma + \mu) + \alpha\xi_2}{\sigma\alpha} I. \tag{2.1.8}$$

Substituting Equation (2.1.8) into Equation (2.1.3), we obtain

$$I = 0, \qquad \text{or} \qquad \beta_E(E)\frac{\omega}{\alpha}S + \beta_I(I)S + \beta_V(V)\frac{\xi_1\omega + \alpha\xi_2}{\alpha\sigma}S - \frac{(\alpha + \mu)\omega}{\alpha} = 0.$$

Now, for $I = 0$, we have $E = 0$, $R = 0$, $V = 0$ and $S = \frac{\wedge}{\mu}$. Replacing the compartment (S, E, I, R, V) at equilibrium state to be defined by $(S_0, E_0, I_0, R_0, V_0)$, thus, the disease-free equilibrium E_f is:

$$(S_0, I_0, E_0, R_0, V_0) = (\frac{\wedge}{\mu}, 0, 0, 0, 0)$$

□

Now we consider the infection to be greater than zero ($I > 0$) such that $I = \overline{I} > 0$, with an objective of showing an existence of **endemic equilibrium**. Now solving the system of Equation (2.1.3)-(2.1.7) leads to fixed points,

$$E = \frac{\omega + \gamma + \mu}{\alpha} I, \qquad R = \frac{\gamma}{\mu} I, \quad \text{and} \quad V = \frac{\xi_1(\omega + \gamma + \mu) + \alpha\xi_2}{\sigma\alpha} I.$$

Simplifying Equation (2.1.3) to find S,

$$(\beta_E(E)ES + \beta_I(I)IS + \beta_V(V)VS = (\alpha + \mu)E. \tag{2.1.9}$$

Then, substitute Equation (2.1.9) into Equation (2.1.4) yields,

$$S = \frac{1}{\mu}(\wedge - (\alpha + \mu)E). \tag{2.1.10}$$

Therefore, substituting E from Equations (2.1.8) into Equation (2.1.10), we get:

$$S = \frac{1}{\mu\sigma}\left((\wedge - (\alpha+\mu))(\omega+\gamma+\mu)\right) I. \tag{2.1.11}$$

Therefore, replacing (S, E, I, R, V) with $(\overline{S}, \overline{E}, \overline{I}, \overline{R}, \overline{V})$ to denote the fixed point which determines the endemic equilibrium, we then have:

$$\begin{aligned}
\overline{E} &= \frac{\omega+\gamma+\mu}{\alpha}\overline{I},\\
\overline{R} &= \frac{\gamma}{\mu}\overline{I},\\
\overline{V} &= \frac{\xi_1(\omega+\gamma+\mu)+\alpha\xi_2}{\sigma\alpha}\overline{I},\\
\overline{S} &= \frac{1}{\mu\sigma}\left((\wedge - (\alpha+\mu))(\omega+\gamma+\mu)\right)\overline{I}.
\end{aligned} \tag{2.1.12}$$

To obtain the **equilibria** for the System (2.1.1) from Equation (2.1.11), we can write S as the function of I as follows:

$$S = \psi(I) = \frac{1}{\mu}\left(\wedge - (\alpha+\mu)\frac{\omega+\gamma+\mu}{\alpha}I\right). \tag{2.1.13}$$

Solving Equation (2.1.11) for $\wedge$, and for simplicity letting $\varphi_1 = \omega+\gamma+\mu$,

$$\wedge = \mu S + (\alpha+\mu)\left(\frac{\varphi_1}{\alpha}\right) I. \tag{2.1.14}$$

Substituting Equation (2.1.14) into Equation (2.1.4) solving for function S, we then have:

$$\begin{aligned}
&\mu S + (\alpha+\mu)\left(\frac{\varphi_1}{\alpha}\right) I - \beta_E(E)SE - \beta_I(I)SI - \beta_V(V)SV - \mu S = 0,\\
&(\alpha+\mu)\left(\frac{\varphi_1}{\alpha}\right) I = \beta_E(E)SE + \beta_I(I)SI + \beta_V(V)SV.
\end{aligned}$$

Substituting the values of E and V, we then have:

$$\begin{aligned}
(\alpha+\mu)\left(\frac{\varphi_1}{\alpha}\right) I &= SI\left[\beta_E\left(\frac{\varphi_1}{\alpha}I\right)\left(\frac{\varphi_1}{\alpha}\right) + \beta_I(I) + \beta_V\left(\frac{\xi_1\varphi_1+\alpha\xi_2}{\sigma\alpha}I\right)\left(\frac{\xi_1\varphi_1+\alpha\xi_2}{\sigma\alpha}\right)\right],\\
S &= (\alpha+\mu)\left(\beta_E\left(\frac{\varphi_1}{\alpha}I\right) + \frac{\alpha}{\varphi_1}\beta_I(I) + \left(\frac{\xi_1\varphi_1+\alpha\xi_2}{\sigma\varphi_1}\right)\beta_V\left(\frac{\xi_1\varphi_1+\alpha\xi_2}{\sigma\alpha}I\right)\right)^{-1},
\end{aligned}$$

$$S = \Psi(I) = (\alpha+\mu)\left(\beta_E\left(\frac{\varphi_1}{\alpha}I\right) + \frac{\alpha}{\varphi_1}\beta_I(I) + \left(\frac{\xi_1\varphi_1+\alpha\xi_2}{\sigma\varphi_1}\right)\beta_V\left(\frac{\xi_1\varphi_1+\alpha\xi_2}{\sigma\alpha}I\right)\right)^{-1},$$

So, considering S as curves $\Phi(I)$, $I>0$ and $\Psi(I)$, $I>0$. From the assumptions $\beta_E(E)>0, \beta_I(I)>0, \beta_V(V)>0$ then, one can notice that $\Psi(I)$ function is strictly decreasing while $\Psi(I)$ function is increasing. Thus, these functions intersect in $\mathbb{R}^2_+$ which determine the equilibria (Yang and Wang, 2020).

2.2 The SEAIHR model of Anguelov et al. (2020)

2.2.1 SEAIHR continuous model.

This model describes the epidemiology dynamics of infection of the COVID-19, which contains six compartments including Death $D(t)$ Susceptible $S(t)$, Exposed $E(t)$, Asymptomatic or mild symptomatic $A(t)$, Infected $I(t)$, Hospitalization $H(t)$ and Recovery $R(t)$ (R_A and R_{IH}). This model not only focuses on the confirmed cases by healthcare centres but considers the asymptomatic cases A, where these individuals are not included on the health centres records/database. In this model (Anguelov et al., 2020), we only considered the transmission of the coronavirus through human-human routes, where a susceptible individual may contract the disease through interaction with the contaminated individual, infectious but asymptomatic individual, or with an infectious and symptomatic individual.

As showed in Figure 2.1, the process between the compartments is the same with Figure 2.2, the only difference is the parameters and the changes or additional classes. A susceptible individual is exposed at a rate of βc, which are either contracted with an infectious but asymptomatic individual or with an infectious and symptomatic individual at some constant $(1-\rho)\sigma$ or become infected by a factor $\rho\sigma$. The asymptomatic individual recover at a rate γ_A, while the infected recover at a rate γ_I or hospitalized at rate δ_I. The individuals in H compartment recover at a rate γ_H. The parameters α_I and α_H are (death rate) of individuals resulted from death in compartment I and H respectively.

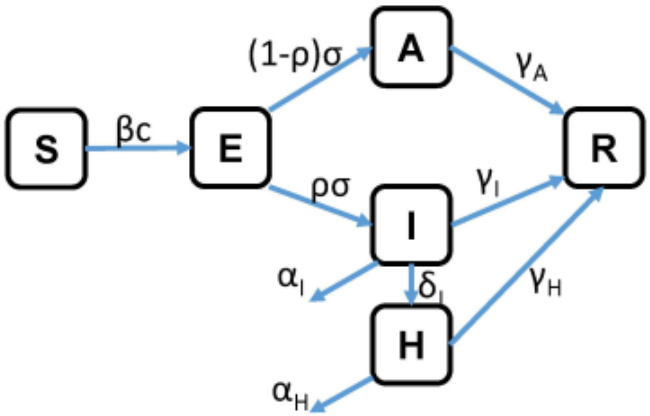

Figure 2.2: Compartment flow representation for the SEAIHR model. Boxes represents epidemiological classes and arrows identify the processes governing transitions between classes (Anguelov et al., 2020).

The mathematical representation of this newly developed model uses a system of six-coupled ordinary differential equations, but in the system, the death compartment $D(t)$ is included which may result from an I and H individual as shown in Figure 2.2. The SEAIHR mathematical model representation

is given by,

$$\begin{aligned}
\frac{dS}{dt} &= -\beta c(I+A)S - \lambda(t)S,\\
\frac{dE}{dt} &= \beta c(I+A)S + \lambda(t)S - \sigma E,\\
\frac{dA}{dt} &= (1-\rho)\sigma E - \gamma_A A,\\
\frac{dI}{dt} &= \rho\sigma E - (\delta_I + \alpha_I + \gamma_I)I,\\
\frac{dH}{dt} &= \delta_I I - (\alpha_H + \gamma_H)H,\\
\frac{dR_A}{dt} &= \gamma_A A\\
\frac{dR_{IH}}{dt} &= \gamma_I I + \gamma_H H,\\
\frac{dD}{dt} &= \alpha_I I + \alpha_H H,
\end{aligned} \tag{2.2.1}$$

where the parameter βc represents the transmission rates of infection ($\beta-$probability of infection, $c-$ number of contacts per person), λ is a function of time accounting infection resulted from individual who traveled abroad, σ is an incubation period, δ_I represents the transfer rate of infected individuals into the hospital, γ is a recovery rate, α represents death rate either from A or I compartment and ρ indicate the ratio of the split of output for an exposed individual between A and I compartment (Anguelov et al., 2020).

Anguelov et al. (2020) assumed that,

- The initial value for the asymptomatic or mild symptomatic cases for this model to be 300, since individuals in this compartment are not recorded in the healthcare database.
- The influx of infective South Africans returning from abroad represented by $\lambda(t)$ until the lock-down came into effect is,

$$\lambda(t) = \begin{cases} 2.18\text{x}10^{-8} & \text{for } t \in [0,8],\\ 0 & \text{for } t \geq 9. \end{cases}.$$

3 Theorem. *Let the compartment of classes $S(t)$, $E(t)$, $A(t)$, $I(t)$, $H(t)$, $R(t)$, $D(t)$ be solution to System (2.2.1), which is satisfied by conditions and assumptions discussed for this model. Then all the compartment with respect to t are all non-negative and bounded for all $t \geq 0$ (Xu and Geng, 2017).*

3. Proposed Nonstandard Finite Difference Schemes for COVID-19

In this chapter, we construct NSFD schemes of two continuous models introduced and discussed in Section 2. We further look at the positivity property for each method which is very essential when dealing with ODE models arising in populations biology, where the state variables representing the sub-populations never take negative values. We discretize these systems following the generalized first-order forward method (Obaid et al., 2017), as shown in Definition 1.

3.1 Consistency and Convergence

3.1.1 Positivity.

The NSFD method is said to be positive, if for any value of the step-size h and $y(t_0) \in \mathbb{R}^n_+$, and its solution remains positive, that is $y_{k+1} \in \mathbb{R}^n_+, \forall k \in \mathbb{N}$ (Dimitrov and Kojouharov, 2008).

3.1.2 Stability.

The FD equation of the form $y_{k+1} = F(h, y_k)$ is said to be elementary stable, for any value of the step size h, if the local stability properties $\overline{y}$ and y^* for the system of ODE and NSFD are the same. Furthermore, if the fixed points y^* of the discrete method is the same as the fixed points $\overline{y}$ of ODE system (Sunday and Agbataobi, 2019). The decay equation which defines a dynamical system on interval $(0, \infty)$ with an asymptotically stable fixed point at $u = 0$ (Anguelov et al., 2020). Using the value of $a = 3$ with $h = 0.5$ in Example 1, the NSFD scheme of decay equation was found to be stable.

3.1.3 Consistency.

The NSFD schemes are consistent with the differential systems if it is stable and positive by or simply a method is consistent if the provided discretization of the differential operators better estimates the derivatives as time or step size approaches zero (Blazek, 2015).

3.1.4 Convergence.

A one-step FD scheme approximating a continuous system, is convergent if approximate solutions approaches or converge to the theoretical or exact solution of the continuous equation as spacing or time step size between discrete samples approaches zero.

This is true if the following conditions hold,

$$u_i^n = \overline{u}(y_i, t_n) \quad \text{as} \quad \Delta y, \Delta t \to 0,$$

where $\overline{u}(y_i, t_n)$ is the solution of the system of continuous equations.

According to the Fundamental theorem of Numerical Analysis from Strang and Freund (1986),

$$\text{consistency} + \text{stability} \Leftrightarrow \text{convegence}.$$

Furthermore, following this, Randall (2007) mentioned that the convergence is a study of global error (E_g) obtained from the relation of local error which determines the stability of finite difference, and the FD is said to be convergent if $||E_g^h|| \to 0$ as $h \to 0$.

We set the time domain which is subdivided through the discrete-time levels $[0, T]$ and $t \to t_k = hk$

where $h = \Delta t > 0$ is time-step size. We then have $(S(t), E(t), I(t), R(t), V(t)) \to (S_k, E_k, I_k, R_k, V_k) \in \mathbb{C}^k\mathbb{R}$.

3.2 The NSFD scheme for SEIR

We discretize the continuous model SEIR, following the generalized first-order forward method as approached by Mickens (2010) , as showed in Definition 1.

3.2.1 Formulation.

From, (1.3.1), the FD for SEIR models can be transformed into

$$\begin{aligned}
\frac{S_{k+1} - S_k}{\phi_1(h)} &= \wedge - (\beta_E(E)E_k + \beta_I(I)I_k + \beta_V(V)V_k + \mu)S_{k+1}, \\
\frac{E_{k+1} - E_k}{\phi_2(h)} &= (\beta_E(E)E_k + \beta_I(I)I_k + \beta_V(V)V_k)S_{k+1} - (\alpha + \mu)E_{k+1}, \\
\frac{I_{k+1} - I_k}{\phi_3(h)} &= \alpha E_{k+1} - (\omega + \gamma + \mu)I_{k+1}, \\
\frac{R_{k+1} - R_k}{\phi_4(h)} &= \gamma I_{k+1} - \mu R_{k+1}, \\
\frac{V_{k+1} - V_k}{\phi_5(h)} &= \xi_1 E_k + \xi_2 I_k - \sigma V_{k+1},
\end{aligned} \tag{3.2.1}$$

where the denominator functions are given by,

$$\begin{aligned}
\phi_1(h) = \phi_4(h) &= \frac{e^{\mu h} - 1}{\mu}, \\
\phi_2(h) &= \frac{e^{(\alpha+\mu)h} - 1}{\alpha + \mu}, \\
\phi_3(h) &= \frac{e^{(\omega+\gamma+\mu)h} - 1}{\omega + \gamma + \mu}, \\
\phi_5(h) &= \frac{e^{\sigma h} - 1}{\sigma}.
\end{aligned} \tag{3.2.2}$$

3.2.2 Equilibrium analysis.

Proving the existence of disease-free equilibrium using the NSFDs for SEIR model, with the infection $I = 0$ which has $I_k = I_{k+1} = 0$, where all the compartment which comprises of the infections are zero, thus the population comprises of susceptible individual (Bawa et al., 2013). For the fixed point of a discrete model, we set $S_{k+1} = S_k = S^*$, $E_{k+1} = E_k = E^*$, $I_{k+1} = I_k = I^*$, $R_{k+1} = R_k = R^*$, $V_{k+1} = V_k = V^*$.

4 Theorem. *A disease-free equilibrium state of SEIR model exists at the point*

$$E_f = (S_0, E_0, I_0, R_0, V_0) = (\frac{\wedge}{\mu}, 0, 0, 0, 0).$$

Proof. In Equation (2.1.1), we set

$$\frac{dS}{dt} = \frac{dE}{dt}, \frac{dI}{dt} = \frac{dR}{dt} = \frac{dV}{dt} = 0.$$

Then,

$$\wedge - (\beta_E(E)E^* + \beta_I(I)I^* + \beta_V(V)V^* + \mu)S^* = 0, \tag{3.2.3}$$
$$(\beta_E(E)E^* + \beta_I(I)I^* + \beta_V(V)V^*)S^* - (\alpha + \mu)E^* = 0, \tag{3.2.4}$$
$$\alpha E^* - (\omega + \gamma + \mu)I^* = 0, \tag{3.2.5}$$
$$\gamma I^* - \mu R^* = 0, \tag{3.2.6}$$
$$\xi_1 E^* + \xi_2 I^* - \sigma V^* = 0, \tag{3.2.7}$$
$$(\beta_E(E)E^* + \beta_V(V)V^*)S^* = (\alpha + \mu)E^*. \tag{3.2.8}$$

Solving Equations (3.2.5), (3.2.6) and (3.2.7), we have:

$$E^* = \frac{\omega + \gamma + \mu}{\alpha} I^*, \qquad R^* = \frac{\gamma}{\mu} I^*, \quad \text{and} \quad V^* = \frac{\xi_1(\omega + \gamma + \mu) + \alpha\xi_2}{\sigma\alpha} I^*. \tag{3.2.9}$$

Substituting Equation (3.2.9) into Equation (3.2.4), we obtain:

$$I^* = 0, \qquad \text{or} \qquad \beta_E(E^*)\frac{\omega}{\alpha}S^* + \beta_I(I^*)S^* + \beta_V(V^*)\frac{\xi_1\omega + \alpha\xi_2}{\alpha\sigma}S^* - \frac{(\alpha + \mu)\omega}{\alpha} = 0.$$

Now, for $I^* = 0$, we have $E^* = 0$, $R^* = 0$, $V^* = 0$ and $S^* = \frac{\wedge}{\mu}$. Replacing the compartment $(S^*, E^*, I^*, R^*, V^*)$ at equilibrium state to be defined by $(S_0^*, E_0^*, I_0^*, R_0^*, V_0^*)$, the disease-free equilibrium E_f is:

$$(S_0^*, I_0^*, E_0^*, R_0^*, V_0^*) = (\frac{\wedge}{\mu}, 0, 0, 0, 0).$$

□

Now we find the **endemic equilibrium** (where $I > 0$) of System (3.2.1). Solving system of Equations from (3.2.3)-(3.2.8), we get:

$$E^* = \frac{\omega + \gamma + \mu}{\alpha} I^*, \qquad R^* = \frac{\gamma}{\mu} I^*, \quad \text{and} \quad V^* = \frac{\xi_1(\omega + \gamma + \mu) + \alpha\xi_2}{\sigma\alpha} I^*.$$

Simplifying Equation (3.2.4) to find S.

$$(\beta_E(E^*)E^*S^* + \beta_I(I^*)I^*S^* + \beta_V(V^*)V^*S^* = (\alpha + \mu)E^*. \tag{3.2.10}$$

Then, substituting Equation (3.2.10) into Equation (3.2.3) yields,

$$S^* = \frac{1}{\mu}(\wedge - (\alpha + \mu)E^*). \tag{3.2.11}$$

Therefore, substituting E^* from Equations (3.2.9) into Equation (3.2.11), we get:

$$S^* = \frac{1}{\mu\sigma}\left((\wedge - (\alpha+\mu))(\omega+\gamma+\mu)\right) I^*. \tag{3.2.12}$$

The fixed point which determines the endemic equilibrium of NSFD scheme for SEIR model are given as

$$\begin{aligned} E^* &= \frac{\omega+\gamma+\mu}{\alpha} I^*, \\ R^* &= \frac{\gamma}{\mu} I^*, \\ V^* &= \frac{\xi_1(\omega+\gamma+\mu)+\alpha\xi_2}{\sigma\alpha} I^*, \\ S^* &= \frac{1}{\mu\sigma}\left((\wedge - (\alpha+\mu))(\omega+\gamma+\mu)\right) I^*, \end{aligned} \tag{3.2.13}$$

which are the same to that of continuous System (2.1.12). Note that the parameters $(\mu, \gamma, \omega, \sigma, \alpha)$ are taken to be positive and considering Conditions (2.1.2).

To obtain the **equilibria** for System (3.2.1), from Equation (3.2.12) we can write S^* as the function of I^* as follows:

$$S^* = \psi(I^*) = \frac{1}{\mu}\left(\wedge - (\alpha+\mu)\frac{\omega+\gamma+\mu}{\alpha} I^*\right). \tag{3.2.14}$$

Solving Equations (3.2.12) for $\wedge$, and for simplicity, letting $\varphi_1 = \omega+\gamma+\mu$, we have:

$$\wedge = \mu S^* + (\alpha+\mu)\left(\frac{\varphi_1}{\alpha}\right) I^*. \tag{3.2.15}$$

Substituting Equation (3.2.15) into Equation (3.2.3) to solve for the function $S*$, we then have:

$$\begin{aligned} &\mu S^* + (\alpha+\mu)\left(\frac{\varphi_1}{\alpha}\right) I^* - \beta_E(E^*)S^*E^* - \beta_I(I^*)S^*I^* - \beta_V(V^*)S^*V^* - \mu S^* = 0, \\ &(\alpha+\mu)\left(\frac{\varphi_1}{\alpha}\right) I^* = \beta_E(E^*)S^*E^* + \beta_I(I^*)S^*I^* + \beta_V(V^*)S^*V^*. \end{aligned}$$

Substituting the values of E^* and V^*, we then have:

$$\begin{aligned} (\alpha+\mu)\left(\frac{\varphi_1}{\alpha}\right) I^* &= S^*I^*\left[\beta_E\left(\frac{\varphi_1}{\alpha}I^*\right)\left(\frac{\varphi_1}{\alpha}\right) + \beta_I(I) + \beta_V\left(\frac{\xi_1\varphi_1+\alpha\xi_2}{\sigma\alpha}I^*\right)\left(\frac{\xi_1\varphi_1+\alpha\xi_2}{\sigma\alpha}\right)\right], \\ S^* &= (\alpha+\mu)\left(\beta_E\left(\frac{\varphi_1}{\alpha}I^*\right) + \frac{\alpha}{\varphi_1}\beta_I(I^*) + \left(\frac{\xi_1\varphi_1+\alpha\xi_2}{\sigma\varphi_1}\right)\beta_V\left(\frac{\xi_1\varphi_1+\alpha\xi_2}{\sigma\alpha}I^*\right)\right)^{-1}, \end{aligned}$$

$$S^* = \Psi(I^*) = (\alpha+\mu)\left(\beta_E\left(\frac{\varphi_1}{\alpha}I^*\right) + \frac{\alpha}{\varphi_1}\beta_I(I^*) + \left(\frac{\xi_1\varphi_1+\alpha\xi_2}{\sigma\varphi_1}\right)\beta_V\left(\frac{\xi_1\varphi_1+\alpha\xi_2}{\sigma\alpha}I^*\right)\right)^{-1}. \tag{3.2.16}$$

If we consider S^* from Solution (3.2.14) and (3.2.16) as curves then, $\Psi(I^*)$, and $\Psi(I^*)$ are functions of Infection, where $I^* > 0$. From the assumptions $\beta_E(E) > 0, \beta_I(I^*) > 0, \beta_V(V) > 0$ then, one can notice that $\Psi(I^*)$ function is strictly decreasing while $\Psi(I^*)$ function is increasing. Thus, these function they intersect in $\mathbb{R}^2_+$ which determine the equilibria (Yang and Wang, 2020).

3.2.3 Positivity.

According to Subsection 3.1.1, we examine the positivity property for this scheme. To do that, we first try to simplify System (3.2.1) by letting

$$\eta = \beta_E(E)E_k + \beta_I(I)I_k + \beta_V(V)V_k + \mu.$$

System (3.2.1) becomes

$$\frac{S_{k+1} - S_k}{\phi_1} = \wedge - \eta S_{k+1}, \tag{3.2.17}$$

$$\frac{E_{k+1} - E_k}{\phi_2} = (\eta - \mu)S_{k+1} - (\alpha + \mu)E_{k+1}, \tag{3.2.18}$$

$$\frac{I_{k+1} - I_k}{\phi_3} = \alpha E_{k+1} - (\omega + \gamma + \mu)I_{k+1}, \tag{3.2.19}$$

$$\frac{R_{k+1} - R_k}{\phi_4} = \gamma I_{k+1} - \mu R_{k+1}, \tag{3.2.20}$$

$$\frac{V_{k+1} - V_k}{\phi_5} = \xi_1 E_k + \xi_2 I_k - \sigma V_{k+1}. \tag{3.2.21}$$

Solving the transformed Equation (3.2.17), we then obtain:

$$\begin{aligned}
\frac{S_{k+1} - S_k}{\phi_1(h)} &= \wedge - \eta S_{k+1}, \\
S_{k+1} - S_k &= \phi_1(h) \wedge -\phi_1(h)\eta S_{k+1}, \\
S_{k+1} + \phi_1(h)\eta S_{k+1} &= \phi_1(h) \wedge + S_k, \\
S_{k+1}(1 + \phi_1(h)\eta) &= \phi_1(h) \wedge + S_k,
\end{aligned}$$

$$\therefore S_{k+1} = \frac{\phi_1(h) \wedge + S_k}{1 + \phi_1(h)\eta}.$$

From Equation (3.2.18), we find that the value E_{k+1} is

$$\begin{aligned}
\frac{E_{k+1} - E_k}{\phi_2(h)} &= (\eta - \mu)S_{k+1} - (\alpha + \mu)E_{k+1}, \\
E_{k+1} - E_k &= \phi_2(h)(\eta - \mu)S_{k+1} - \phi_2(h)(\alpha + \mu)E_{k+1}, \\
E_{k+1} + \phi_2(h)(\alpha + \mu)E_{k+1} &= \phi_2(h)(\eta - \mu)S_{k+1} + E_k, \\
E_{k+1}(1 + \phi_2(h)(\alpha + \mu)) &= \phi_2(h)(\eta - \mu)S_{k+1} + E_k,
\end{aligned}$$

$$\therefore E_{k+1} = \frac{\phi_2(h)(\eta - \mu)S_{k+1} + E_k}{1 + \phi_2(h)(\alpha + \mu)}.$$

Solving Equation (3.2.19), we have:

$$\begin{aligned}
\frac{I_{k+1}-I_k}{\phi_3(h)} &= \alpha E_{k+1} - (\omega+\gamma+\mu)I_{k+1},\\
I_{k+1}-I_k &= \phi_3(h)\alpha E_{k+1} - \phi_3(h)(\omega+\gamma+\mu)I_{k+1},\\
I_{k+1}+\phi_3(h)(\omega+\gamma+\mu)I_{k+1} &= \phi_3(h)\alpha E_{k+1} + I_k,\\
I_{k+1}(1+\phi_3(h)(\omega+\gamma+\mu)) &= \phi_3(h)\alpha E_{k+1} + I_k,\\
\therefore I_{k+1} &= \frac{\phi_3(h)\alpha E_{k+1}+I_k}{1+\phi_3(h)(\omega+\gamma+\mu)}.
\end{aligned}$$

Solving Equation (3.2.20), we obtain:

$$\begin{aligned}
\frac{R_{k+1}-R_k}{\phi_4(h)} &= \gamma I_{k+1} - \mu R_{k+1},\\
R_{k+1}-R_k &= \phi_4(h)\gamma I_{k+1} - \phi_4(h)\mu R_{k+1},\\
R_{k+1}+\phi_4(h)\mu R_{k+1} &= \phi_4(h)\gamma I_{k+1} + R_k,\\
R_{k+1}(1+\phi_4(h)\mu) &= \phi_4(h)\gamma I_{k+1} + R_k,\\
\therefore R_{k+1} &= \frac{R_k+\phi_4(h)\gamma I_{k+1}}{(1+\phi_4(h)\mu)}.
\end{aligned}$$

Solving Equation (3.2.21), we get:

$$\begin{aligned}
\frac{V_{k+1}-V_k}{\phi_5(h)} &= \xi_1 E_k + \xi_2 I_k - \sigma V_{k+1},\\
V_{k+1}(1+\sigma) &= \phi_5(h)(\xi_1 E_k + \xi_2 I_k) + V_k,
\end{aligned}$$

$$V_{k+1} = \frac{\phi_5(h)(\xi_1 E_k + \xi_2 I_k)+V_k}{1+\sigma}.$$

The system of equations from (3.2.17) - (3.2.21) give the following solution:

$$\begin{aligned}
S_{k+1} &= \frac{\phi_1(h) \wedge + S_k}{1+\phi_1(h)\eta},\\
E_{k+1} &= \frac{\phi_2(h)(\eta-\mu)S_{k+1}+E_k}{1+\phi_2(h)(\alpha+\mu)},\\
I_{k+1} &= \frac{\phi_3(h)\alpha E_{k+1}+I_k}{1+\phi_3(h)(\omega+\gamma+\mu)},\\
R_{k+1} &= \frac{R_k+\phi_4(h)\gamma I_{k+1}}{(1+\phi_4(h)\mu)},\\
V_{k+1} &= \frac{\phi_5(h)(\xi_1 E_k+\xi_2 I_k)+V_k}{1+\sigma},
\end{aligned} \tag{3.2.22}$$

with $\eta = \beta_E(E)E_k + \beta_I(I)I_k + \beta_V(V)V_k + \mu$.

Consider Assumptions (2.1.2) that $\beta_E(E), \beta_I(I), \beta_V(V)$ are positive. If $S_k \geq 0, I_k \geq 0, E_k \geq 0, R_k \geq 0$ and $V_k \geq 0$, following Theorem 1, it implies that S_{k+1} and V_{k+1} are positive values. If the values of S_{k+1}, η and E_k are used, they give the non-negative value for E_{k+1}, applying the value of E_{k+1} and I_k it also gives the positive value for I_{k+1} and it follows that R_{k+1} is a non-negative value by taking R_k and I_{k+1}. Therefore, we can conclude that the values for $S_{k+1}, E_{k+1}, I_{k+1}, R_{k+1}$ and V_{k+1} are positive, which is what we expected or stated from Subsection 3.1.1.

3.3 Summary

We showed that the NSFD scheme has the same fixed point as the continuous model for the case of $I > 0$ and having the same equilibria. Thus, by Subsection 3.1.2, this implies that the discrete method is elementary stable. Furthermore, we proved that the discrete method is positive using Theorem 1 and Subsection 3.1.1. Then, since the discrete method is elementary stable, it can be concluded that it is dynamically consistent with the model. According to Subsection 3.1.4 that the scheme must approximate the solution approaching the exact solution as $h \to 0$, since the scheme is stable, DC and positive all the time, it can be concluded that the discrete method approximate well and converges to the exact solution as step size tends to zero.

3.4 The NSFD scheme for SEAIHR

We discretize the continuous model SEAIHR, following the generalized first-order forward method as approached by Mickens (2010).

3.4.1 Formulation.

The discretization of SEAIHR using Definition 1, is given by

$$
\begin{aligned}
\frac{S_{k+1} - S_k}{\psi_1(h)} &= -\beta c(I_k + A_k)S_{k+1} - \lambda(t)S_{k+1}, \\
\frac{E_{k+1} - E_k}{\psi_2(h)} &= \beta c(I_k + A_k)S_{k+1} + \lambda(t)S_{k+1} - \sigma E_{k+1}, \\
\frac{A_{k+1} - A_k}{\psi_3(h)} &= (1-\beta)\sigma E_{k+1} - \gamma_A A_{k+1}, \\
\frac{I_{k+1} - I_k}{\psi_4(h)} &= \rho\sigma E_{k+1} - (\delta_I + \alpha_I + \gamma_I)I_{k+1}, \\
\frac{H_{k+1} - H_k}{\psi_5(h)} &= \delta_I I_{k+1} - (\alpha_H + \gamma_H)H_{k+1}, \\
\frac{R_{A_{k+1}} - R_{A_k}}{\psi_6(h)} &= \gamma_A A_{k+1}, \\
\frac{R_{IH_{k+1}} - R_{IH_k}}{\psi_7(h)} &= \gamma_I I_{k+1} + \gamma_H H_{k+1}, \\
\frac{D_{k+1} - D_k}{\psi_8(h)} &= \alpha_I I_{k+1} + \alpha_H H_{k+1},
\end{aligned}
\tag{3.4.1}
$$

where the denominator functions are:

$$\begin{aligned}
\psi_1(h) &= \frac{e^{\lambda_m h}-1}{\lambda_m}, \quad \text{where} \quad \lambda_m = \max_t \lambda(t).\\
\psi_2(h) &= \frac{e^{\sigma h}-1}{\sigma},\\
\psi_3(h) = \psi_6 &= \frac{e^{\gamma_A h}-1}{\gamma_A},\\
\psi_4(h) = \psi_7 &= \frac{e^{(\delta_I+\alpha_I+\gamma_I)h}-1}{\delta_I+\alpha_I+\gamma_I},\\
\psi_5(h) = \psi_8 &= \frac{e^{(\alpha_H+\gamma_H)h}-1}{\alpha_H+\gamma_H},
\end{aligned} \tag{3.4.2}$$

3.4.2 Positivity.

According to Subsection 3.1.1, we examine the positivity property for this scheme, to do that we first try to simplify System (3.2.1).

$$S_{k+1} - S_k = -\psi_1\beta c(I_k + A_k)S_{k+1} - \psi_1\lambda(t)S_{k+1}, \tag{3.4.3}$$
$$E_{k+1} - E_k = \psi_2\beta c(I_k + A_k)S_{k+1} + \psi_2\lambda(t)S_{k+1} - \psi_2\sigma E_{k+1}, \tag{3.4.4}$$
$$A_{k+1} - A_k = (1-\rho)\sigma\psi_3 E_{k+1} - \gamma_A\psi_3 A_{k+1}, \tag{3.4.5}$$
$$I_{k+1} - I_k = \rho\sigma\psi_4 E_{k+1} - \psi_4(\delta_I + \alpha_I + \gamma_I)I_{k+1}, \tag{3.4.6}$$
$$H_{k+1} - H_k = \delta_I\psi_5 I_{k+1} - \psi_5(\alpha_H + \gamma_H)H_{k+1}, \tag{3.4.7}$$
$$R_{A_{k+1}} - R_{A_k} = \gamma_A\psi_3 A_{k+1}, \tag{3.4.8}$$
$$R_{IH_{k+1}} - R_{IH_k} = \psi_4(\gamma_I I_{k+1} + \gamma_H H_{k+1}), \tag{3.4.9}$$
$$D_{k+1} - D_k = \psi_5(\alpha_I I_{k+1} + \alpha_H H_{k+1}). \tag{3.4.10}$$

Solving for Equation (3.4.3), we obtain:

$$\begin{aligned}
S_k &= S_{k+1}(1 + \psi_1\beta c(I_k + A_k) + \lambda(t),\\
S_{k+1} &= \frac{S_k}{1 + \psi_1\beta c(I_k + A_k) + \lambda(t)}.
\end{aligned}$$

Solving for Equation (3.4.4), we get:

$$\begin{aligned}
E_{k+1}(1 + \psi_2\sigma) &= E_k + \psi_2(\lambda(t) + \beta c(I_k + A_k))S_{k+1},\\
E_{k+1} &= \frac{E_k + \psi_2(\lambda(t) + \beta c(I_k + A_k))S_{k+1}}{1 + \psi_2\sigma}.
\end{aligned}$$

Solving Equation (3.4.5) yield

$$\begin{aligned}
A_{k+1}(1 + \psi_3\gamma_A) &= A_k + (1-\rho)\psi_3\sigma E_{k+1},\\
A_{k+1} &= \frac{A_k + (1-\rho)\psi_3\sigma E_{k+1}}{1 + \psi_3\gamma_A}.
\end{aligned}$$

And solving for Equation (3.4.6), we get:

$$\begin{aligned}
I_{k+1}(1 + \psi_4(\delta_I + \alpha_I + \gamma_I)) &= I_k + \rho\psi_4\sigma E_{k+1},\\
I_{k+1} &= \frac{I_k + \rho\psi_4\sigma E_{k+1}}{1 + \psi_4(\delta_I + \alpha_I + \gamma_I)}.
\end{aligned}$$

Solving Equation (3.4.7) yield

$$H_{k+1}(1+\psi_5(\alpha_H+\gamma_H)) = H_k + \psi_5\delta_I I_{k+1},$$
$$H_{k+1} = \frac{H_k + \psi_5\delta_I I_{k+1}}{1+\psi_5(\alpha_H+\gamma_H)}.$$

Solving for Equation (3.4.8), we get:

$$R_{A_{k+1}} = R_{A_k} + \gamma_A\psi_3 A_{k+1}.$$

Solving for Equation (3.4.9), we get:

$$R_{IH_{k+1}} = R_{IH_k} + \psi_4(\gamma_I I_{k+1} + \gamma_H H_{k+1}).$$

Solving Equation (3.4.10), we then obtain:

$$D_{k+1} = D_k + \psi_5(\alpha_I I_{k+1} + \alpha_H H_{k+1}).$$

Therefore, solution of Equation (3.4.1) shows that if $S_k \geq 0$, $E_k \geq 0$, $A_k \geq 0$, $I_k \geq 0$, $H_k \geq 0$, $R_k \geq 0$ and $D_k \geq 0$ using Theorem 3 and applying the parameters which are said to be positive, then $R_{A_{k+1}}$, $R_{IH_{k+1}}$ and D_{k+1} are positive. Using the values of S_k, E_k and A_k, we notice that S_{k+1} is a positive value. Applying S_{k+1}, we get a positive value for E_{k+1}. Taking E_{k+1} and A_k, we observe that A_{k+1} and I_{k+1} are also non-negative value. It follows that H_{k+1} is positive if we take the value of I_{k+1}. We can conclude that S_{K+1}, E_{K+1}, A_{k+1}, I_{k+1}, H_{k+1}, R_{k+1} and D_{k+1} are all positive values, which is what we expected or stated from the Subsection 3.1.1.

3.5 Summary

According to the discussion in Subsection 3.1.1, the discretization method for SEAIHR model is proved to be positive in all cases using the model assumptions and Theorem 3. Sunday and Agbataobi (2019) said that the scheme is DC if its elementary stable and if the positivity property hold true. Since it is stable and consistent then the approximated solution converges to the exact solution, concluding that NSFD scheme for SEAIHR model is convergent as the step size approaches zero.

4. Numerical Analysis and Simulations

4.1 SEIR analysis

The SEIR model was developed and applied in China by Yang and Wang (2020), in 2020, describing the transmission dynamics of the COVID-19 epidemic, which incorporate multiple transmission, with some assumptions discussed in Section 2.1.1. The implications of this model and numerical simulations for the coronavirus epidemic were initiated from 23 January 2020 to 10 in February 2020, and at that time the City of Wuhan was placed in quarantine. Taking the initial conditions as $(S(0), E(0), I(0), R(0), V(0)) = (89985051000, 475, 10, 0, 10000)$. To conduct the simulations , three transmission rates in the model were considered.

$$\beta_E(E) = \frac{\beta_{E0}}{1+CE}, \qquad \beta_I(I) = \frac{\beta_{I0}}{1+CI}, \quad \text{and} \quad \beta_V(V) = \frac{\beta_{V0}}{1+CV}. \tag{4.1.1}$$

The numerators are all positive constants, which denote the values of these transmission rates. From the equilibrium analysis of the NSFD scheme, we can have some cases which suggest the intervention strategies targeting all three transmission routes of infection, given by reproduction number $\mathcal{R}_0$. The definition of the constants and parameter values used in the model are given in Table 4.1. The incubation period is ranged between $2-14$ days, where the mean value is $5-7$ days (Yang and Wang, 2020). For this model 7 days was taken to be an incubation period. We fitted the model using the standard least square method, to determine the values of ξ_1 and ξ_2 parameters, hence, we were able to show that $\xi_2 = 0$ while ξ_1 ranges between (0, 23.184). For a value $\xi_2 = 0$ the model still holds, since the contribution of coronavirus term remains a positive value Yang and Wang (2020).

Table 4.1: Definitions and values of parameters Yang and Wang (2020).

Parameter	Definition	Estimated Mean value
$\wedge$	Influx rate	271.23 pe day
β_{E0}	Transmission constant between S and E	$3.11\text{x}10^{-8}$/person/day
β_{I0}	Transmission constant between S and I	$0.62\text{x}10^{-8}$/person/day
β_{V0}	Transmission constant between S and V	$1.03\text{x}10^{-8}$/person/day
c	Transmission adjustment coefficient	$1.01\text{x}10^{-4}$
$1/\alpha$	Incubation Period	7 days
ω	Diseases- Induced death rate	0.01
μ	Natural death rate	$3.01\text{x}10^{-5}$ /day
γ	Recovery rate	1/15 /day
σ	Removal rate of virus	1 /day
ξ_1	Virus shedding by exposed people	2.30 / person /day/ml
ξ_2	Virus shedding by exposed people	0 / person /day/ml

Applying the same parameter values into proposed NSFD scheme Equation (3.2.1) for SEIR model, to describe the transmission dynamics of the COVID-19 epidemic under same assumptions. The curves in Figure 4.1a and 4.1b, continuous model and discrete method respectively reach the maximum values as shown in Table 4.2. It is observable that the NSFD method approximation is almost in agreement with the continuous model, with a small error involved (Khumalo, 2020). After reaching maximum, the

curves shown in Figure 4.1 slowly descend, implying that the rate of infection is decreasing, this may be due to the fact that, the city was already under lockdown, hence the movement and interaction between people was reduced, and as a result it affected the spread of coronavirus or it minimized the probability of one being exposed or infected through human or environment. As time increases (t_0+nh), where $n = 1, 2, 3, ...$, the recovery rate of the infected individuals increases regardless of how the infection occurred between the multiple pathways.

Table 4.2: Maximum values of infected and Exposed.

Models	Exposed individuals	Infected individuals
SEIR	290939758	534007018
NSFD	290901569	541756677

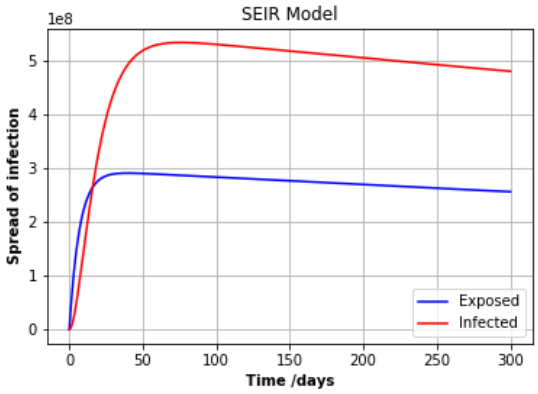

(a) Graph for SEIR model of System (2.1.1)

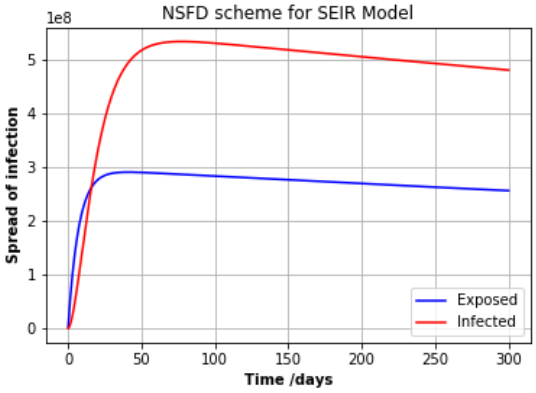

(b) Graph for NSFD scheme of System (3.2.1) for SEIR model

Figure 4.1: The simulation of SEIR for COVID-19 found from Khumalo (2020).

4.2 SEAIHR analysis

The SEAIHR model was developed in South Africa, to study the transmission of coronavirus with a special case: Asymptomatic/symptomatic (A), which is explained in Section 2.2.1, where a susceptible individual may contract the virus through interaction with a contaminated individual, infectious but asymptomatic or with an infectious and symptomatic. In this paper, we use this model to evaluate the pandemic of COVID-19 in South Africa. The first case of coronavirus in South Africa was confirmed on 5 March 2020, where the cases around that time were dominated by the individuals who traveled abroad, this was assumed to be case ranging from 5 March to 20 March 2020. Thus this yields to a function of time used to account for infection brought in by those who traveled abroad $(\lambda(t))$ as

$$\lambda(t) = \begin{cases} 2.18\text{x}10^{-8} & \text{for } t \in [0, 8] \\ 0 & \text{for } t \geq 9 \end{cases}.$$

The initial condition used to simulate the spread for the coronavirus in South Africa is from the data presented or broadcast by WHO. The simulation was initiated on 19 March 2020 and at that time there were only 150 confirmed cases and no recoveries and death from the virus. The asymptomatic value

was assumed to be 300 by Anguelov et al. (2020). The given initial conditions are $(S(0),\ A(0),\ E(0),\ I(0),\ H(0),\ R_A(0),\ R_{IH}(0),\ D(0)) = (59\ 309\ 000,\ 300,\ 0,\ 150,\ 0,\ 0,\ 0,\ 0)$, and the parameters used are shown below in Table 4.3.

Table 4.3: Definitions and values of parameters.

Parameter	Definition	Estimated Mean value
γ_A	Recovery rate of Asymptomatic individual	0.0714
γ_I	Recovery rate of Infected individual	0.0643
γ_H	Recovery rate of Hospitalized individual	0.1
Δ_I	Hospitalization rate	0.00643
α_I	Death rate of Infected individual	$3.57\text{x}10^{-4}$
α_H	Death rate of Hospitalized individual	0.0286
σ	Incubation period	1
ρ	ratio of split of output for exposed individual	0.4
βc	Transmission rate of infection	0.2

Figure 4.2 show graphs of the SEAIHR continuous and discretization model respectively, with infection (I) in the red curve and recovery (from the hospital) in the green curve. According to the data used, the simulation starts on the 19 March 2020 as the origin $(t = 0)$. The curves are of the fitted value of $\beta = 0.2$ and using $\lambda t = 2.18\text{x}10^{-8}$ from Anguelov et al. (2020). After 8 days from 19 March, the government initiated a country lockdown due to the rapid increases of coronavirus, and from Anguelov et al. (2020) the new value of β was fitted from the new data influenced by lockdown, which is 0.07. From the initial point, we expected a very rapid increase in infection, this is due to individuals who are infectious and asymptomatic/symptomatic (A) since they are not part of the confirmed cases (tested and recorded) but able to spread the disease. From these result, the number of the infected individuals will continue to rise until reaching a maximum number of $(22\ 869\ 087)$ using continuous estimation and $(22\ 388\ 212)$ by a discretized method, with a slow increase of recovery cases reaching a maximum of $(1\ 067\ 708)$ by continuous prediction and $(1\ 704\ 103)$ by a discretized method. Thereafter, an infection curve continues in the manner presented, decreasing very slowly. The step size used for Figure 4.2 is $0.002 < h < 0.099$ for discretization model.

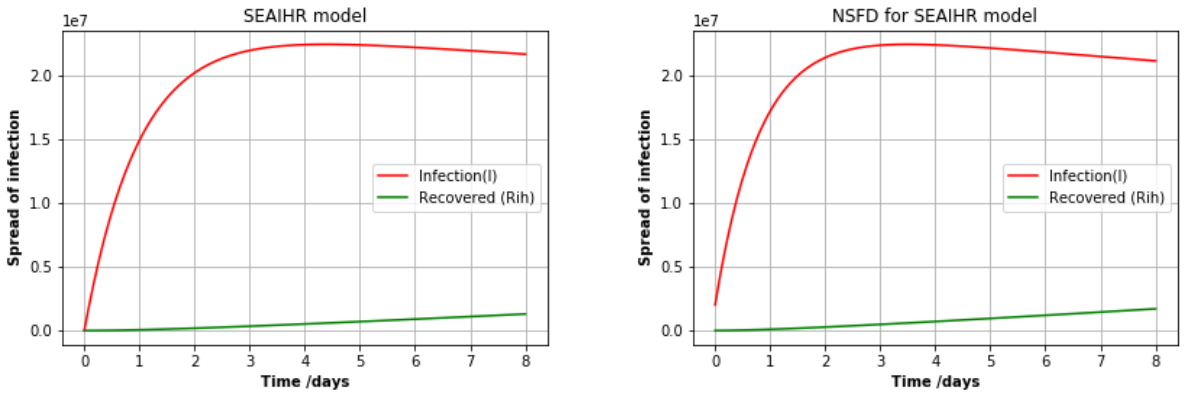

(a) The SEAIHR model of System (2.2.1) (b) Graph for NSFD scheme of System (3.4.1) scheme

Figure 4.2: The simulation of SEAIHR for COVID-19 found from Khumalo (2020)

Figure 4.3 show the curves of deaths, recovered (Ra), and recovered (Rih) using again the continuous and discretization method respectively, where we observe the increase between both recovery curves while deaths also increase but very slowly. The maximum values of D, Ra, Rih presented in Figure 4.3 are $(15,\ 4680,\ 282)$ and $(14,\ 4348,\ 261)$ respectively, still using $\beta = 0.2$ with the step size $0.002 < h < 0.0035$.

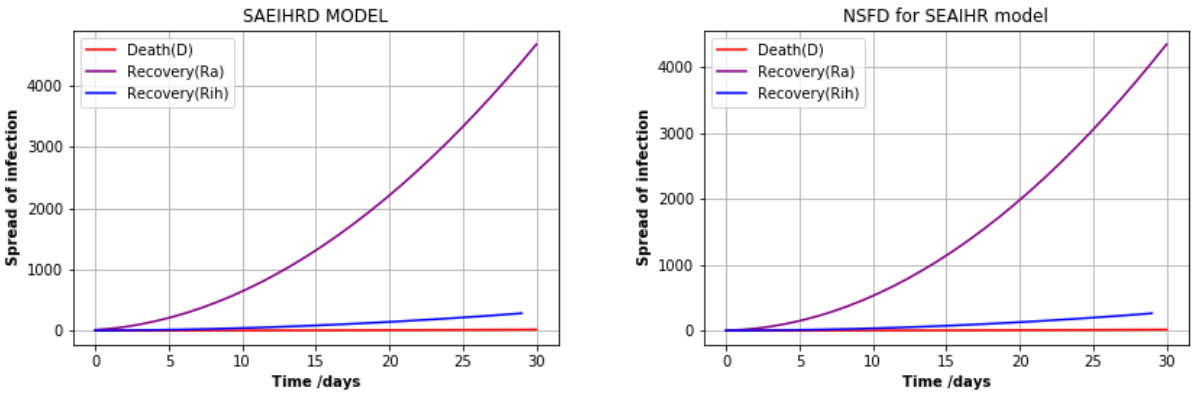

(a) The SEAIHR model (2.2.1)

(b) The NSFD scheme

Figure 4.3: Shows the simulation of SEAIHR for COVID-19 found from Khumalo (2020)

These two methods SEIR and SEAIHR with their NSFD method show the similar behavior for the infection of coronavirus, even though the application of these methods are in different places but with one objective to detect the dynamic spread of the disease. The places have different populations and the methods use different parameters but they show a similar trend. The code for this work can be found in Khumalo (2020)

5. Conclusion

In this paper, we considered SEIR model and SEAIHR model for the transmission dynamics of COVID-19. Both models are made of nonlinear first-order differential equations. We expanded on their presentation as initially seen in (Yang and Wang (2020) and Anguelov et al. (2020)). In these papers, the SEIR and the SEAIHR models were respectively simulated against real COVID-19 data of Wuhan City and South Africa. For the SEIR model, through an equilibrium analysis, we established the infection-free equilibrium and proved the existence of the endemic equilibrium.

We constructed a nonstandard finite difference scheme for each of these models and showed their positivity and stability. For the proposed discrete SEIR, we determined the infection-free equilibrium and proved the existence of an endemic equilibrium. This analysis replicated that obtained for the continuous models (SEIR).

Furthermore, the proposed discrete SEIR and SEAIHR were simulated against real COVID-19 data of Wuhan City and South Africa, respectively. The obtained figures in Section 4 shows that the schemes uphold the continuous models further confirming the dynamical consistency of the proposed discretization.

Future work: we are currently investigating the construction of a fresh nonstandard finite difference scheme for the transmission dynamics of COVID-19 where we consider partial lockdown as a special control measure. We will calibrate the said model on real data from several countries and use it for relative long time predictions.

Acknowledgements

I want to acknowledge AIMS and its funders for supporting this work, as well as my supervisor Prof. Justin Munyakazi from UWC and my Tutor Faraniaina Rasolofoson for their guidance, support from the beginning of my research and for giving me time every day without complaints. I want to acknowledge my family and my Nana for their support and for being understanding.

References

Anguelov, R., Banasiak, J., Bright, C., Lubuma, J., and Ouifki, R. The big unknown: The asymptomatic spread of COVID-19. *BIOMATH*, 9:2005103, 05 2020. doi: 10.11145/j.biomath.2020.05.103.

Barto, A. G. *Discrete and Continuous Models*, pages 377–396. Springer US, Boston, MA, 1991. ISBN 978-1-4899-0718-9. doi: 10.1007/978-1-4899-0718-9_26. URL https://doi.org/10.1007/978-1-4899-0718-9_26.

Batista, M. Estimation of the final size of the COVID-19 epidemic. *medRxiv*, 2020. doi: 10.1101/2020.02.16.20023606. URL https://www.medrxiv.org/content/early/2020/02/28/2020.02.16.20023606.

Bawa, M., Abdulrahman, S., and Adabara, N. Stability analysis of the disease-free equilibrium state for lassa fever disease. *International Journal of Science and Mathematics Education*, 9:115–123, 04 2013.

Blazek, J. Chapter 2 - governing equations. In Blazek, J., editor, *Computational Fluid Dynamics: Principles and Applications (Third Edition)*, pages 7 – 27. Butterworth-Heinemann, Oxford, third edition edition, 2015. ISBN 978-0-08-099995-1. doi: https://doi.org/10.1016/B978-0-08-099995-1.00002-6. URL http://www.sciencedirect.com/science/article/pii/B9780080999951000026.

Dimitrov, D. and Kojouharov, H. Nonstandard finite-difference methods for predator–prey models with general functional response. *Mathematics and Computers in Simulation*, 78:1–11, 06 2008. doi: 10.1016/j.matcom.2007.05.001.

Grassly, C., Nicholas and Fraser, C. Mathematical models of infectious disease transmission. *Nature reviews. Microbiology*, 6, 05 2008. doi: doi:10.1038/nrmicro1845.

Imai, N., Cori, A., Dorigatti, I., Baguelin, M., Donnelly, C., Riley, S., and Ferguson, N. Report 3: Transmissibility of 2019-nCoV. *Imperial College London*, 01 2020. doi: 10.25561/77148. URL http://hdl.handle.net/10044/1/77148.

Khumalo, S. Aims project: Python code for Mathematical models and NSFD scheme for the COVID-19, 2020. URL https://github.com/Sphak/my-project-/blob/master/AIMS%20PROJECT.ipynb.

Li, Q., Guan, X., Wu, P., Wang, X., Zhou, L., Tong, Y., Ren, R., Leung, K., Lau, E., Wong, J. Y., Xing, X., Xiang, N., Wu, Y., Li, C., Chen, Q., Li, D., Liu, T., Zhao, J., Li, M., and Feng, Z. Early transmission dynamics in Wuhan, China, of novel coronavirus–infected pneumonia. *New England Journal of Medicine*, 382, 01 2020. doi: 10.1056/NEJMoa2001316.

Manning, P. M. and Margrave, G. F. Introduction to nonstandard finite difference modelling. *CREWES Research Report*, 18, 08 2020.

Mickens, R. *Nonstandard finite difference methods*, pages 1–9. 10 2005a. doi: 10.1142/9789812703316_0001.

Mickens, R. *A SIR-model with square-root dynamics: an NSFD scheme*, volume 16, pages 209–216. 02 2010. doi: 10.1080/10236190802495311.

Mickens, R. E. *Advances in the Applications of Nonstandard Finite Diffference Schemes*. World Scientific, 2005b.

Muhammad, A., Khan, H., and Owais, M. Strategies to control and prevent novel coronavirus 2019. *Journal of the Liaquat University of Medical and Health Sciences*, 19, 05 2020.

Obaid, H. A., Ouifki, R., and Patidar, K. C. A nonstandard finite difference method for solving a mathematical model of HIV-TB co-infection. *Journal of Difference Equations and Applications*, 23(6): 1105–1132, 2017. doi: 10.1080/10236198.2017.1318859. URL https://doi.org/10.1080/10236198.2017.1318859.

Randall, L. Finite difference methods for ordinary and partial differential equations -steady-state and time-dependent problems. SIAM, 2007. ISBN 0898717833, 9780898717839.

R.Anguelov, J.M.S.Lubuma, and M.Shillor. Topological dynamic consistency of non-standard finite difference schemes for dynamical systems. *Journal of Difference Equations and Applications*, 17(12): 1769–1791, 2011. doi: 10.1080/10236198.2010.488226. URL https://doi.org/10.1080/10236198.2010.488226.

Rao, P., Ratnam, K., and Murthy, M. Stability preserving non standard finite difference schemes for certain biological models. *International Journal of Dynamics and Control*, 6, 12 2018. doi: 10.1007/s40435-018-0410-6.

Rothe, C., Schunk, M., Sothmann, P., Bretzel, G., Froeschl, G., Wallrauch, C., Zimmer, T., Thiel, V., Janke, C., Guggemos, W., Seilmaier, M., Drosten, C., Vollmar, P., Zwirglmaier, K., Zange, S., Wölfel, R., and Hoelscher, M. Transmission of 2019-ncov infection from an asymptomatic contact in germany. *New England Journal of Medicine*, 382, 01 2020. doi: 10.1056/NEJMc2001468.

Strang, G. and Freund, L. B. Introduction to Applied Mathematics. *Journal of Applied Mechanics*, 53 (2):480–480, 06 1986. ISSN 0021-8936. doi: 10.1115/1.3171799. URL https://doi.org/10.1115/1.3171799.

Sunday, J. and Agbataobi, G. A reformulated non-standard finite difference method for the solution of autonomous dynamical differential equations. *ICASTOR Journal of Mathematical Sciences*, 13:1–15, 06 2019.

Thieme, R., Horst. *Mathematics in Population Biology*. Princeton University Press, 2003. doi: 10.2307/j.ctv301f9v. URL http://www.jstor.org/stable/j.ctv301f9v.

Tu, W.-J., Zeb, A., Alzahrani, E., Erturk, S., Vedat, and Zaman, G. Mathematical model for coronavirus disease 2019 COVID-19 containing isolation class. *BioMed Research International*, 2020. ISSN 2314-6133. doi: 10.1155/2020/3452402.

Uddin, M. I., Shah, S. A. A., and Al-Khasawneh, M. A. A novel deep convolutional neural network model to monitor people following guidelines to avoid COVID-19. *Journal of Sensors*, pages 1–15, 07 2020. doi: 10.1155/2020/8856801. URL https://doi.org/10.1155/2020/8856801.

Victor, A. Mathematical predictions for COVID-19 as a glabal pandemic. 03 2020. doi: http://dx.doi.org/10.2139/ssrn.3555879.

Wang, D., Hu, B., Hu, C., Zhu, F., Liu, X., Zhang, J., Wang, B., Xiang, H., Cheng, Z., Xiong, Y., Zhao, Y., Li, Y., Wang, X., and Peng, Z. Clinical characteristics of 138 hospitalized patients with 2019 novel coronavirus–infected pneumonia in Wuhan, China. *JAMA*, 323, 02 2020. doi: 10.1001/jama.2020.1585.

Xu, J. and Geng, Y. Stability preserving NSFD scheme for a delayed viral infection model with cell-to-cell transmission and general nonlinear incidence. *Journal of Difference Equations and Applications*, 23:1–24, 03 2017. doi: 10.1080/10236198.2017.1304933.

Yang, C. and Wang, J. A mathematical model for the novel coronavirus epidemic in Wuhan, China. *Mathematical Biosciences and Engineering*, 17:2708–2724, 03 2020. doi: 10.3934/mbe.2020148.

Yang, Z., Zeng, Z., Wang, K., Wong, S.-S., Liang, W., Zanin, M., Liu, P., Cao, X., Gao, Z., Mai, Z., Liang, J., Liu, X., Li, S., Li, Y., Ye, F., Guan, W., Yang, Y., Li, F., Luo, S., Xie, Y., Liu, B., Wang, Z., Zhang, S., Wang, Y., Zhong, N., and He, J. Modified SEIR and AI prediction of the epidemics trend of COVID-19 in China under public health interventions. *Journal of Thoracic Disease*, 12(3), 2020. ISSN 2077-6624. URL http://jtd.amegroups.com/article/view/36385.

Zhen, W., Bauch, C., Bhattacharyya, S., D'Onofrio, A., Manfredi, P., Perc, M., Perra, N., Salathé, M., and Zhao, D. Statistical physics of vaccination. *Physics Reports*, 664, 08 2016. doi: 10.1016/j.physrep.2016.10.006.